JOC The Journal of Organic Chemistry

Article

pubs.acs.org/joc

Synthesis of 1,2-Bis(2-aryl-1*H*-indol-3-yl)ethynes via 5-*exo*-Digonal Double Cyclization Reactions of 1,4-Bis(2-isocyanophenyl)buta-1,3-diyne with Aryl Grignard Reagents

Rino Ishikawa,[†] Ryosuke Iwasawa,[†] Yuichiro Takiyama,[†] Tomokazu Yamauchi,[‡] Tetsuo Iwanaga,[‡] Makoto Takezaki,[‡] Motonori Watanabe,[§] Naozumi Teramoto,[†] Toshiaki Shimasaki,*[,†] and Mitsuhiro Shibata*[,†]

[†]Department of Applied Chemistry, Faculty of Engineering, Chiba Institute of Technology, 2-17-1 Tsudanuma, Narashino, Chiba 275-0016, Japan

[‡]Department of Chemistry, Faculty of Science, Okayama University of Science, 1-1 Ridaicho, Kita-ku, Okayama 700-0005, Japan

[§]International Institute for Carbon-Neutral Energy Research (I2CNER), Molecular Photoconversion Devices Division, Kyushu University, 744 Motooka, Nishi-ku, Fukuoka 819-0395, Japan

Supporting Information

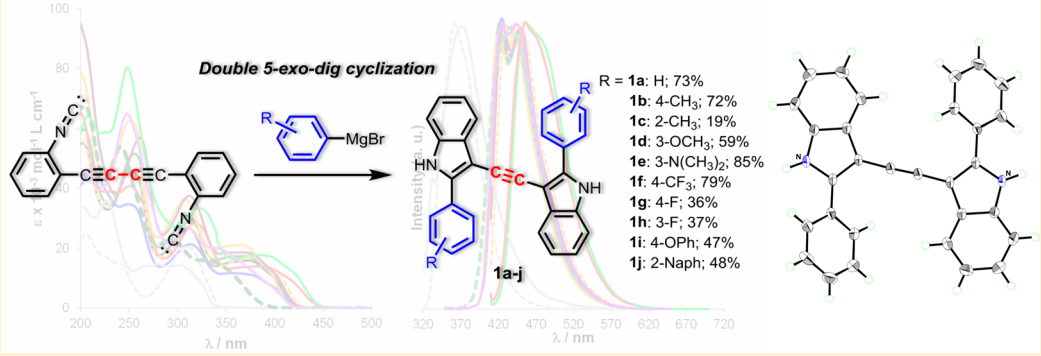

ABSTRACT: New π-conjugated 1,2-bis(2-aryl-1*H*-indol-3-yl)ethynes **1a−j** having various substituents on the two aryl groups were efficiently synthesized via unusual 5-*exo*-digonal double isocyanide-acetylene cyclization reactions of 1,4-bis(2-isocyanophenyl)buta-1,3-diyne **3** and aryl Grignard reagents (R-MgBr, R = C_6H_5 (**1a**), 4-$H_3CC_6H_4$ (**1b**), 2-$H_3CC_6H_4$ (**1c**), 3-$MeOC_6H_4$ (**1d**), 3-$(CH_3)_2NC_6H_4$ (**1e**), 4-$F_3CC_6H_4$ (**1f**), 4-FC_6H_4 (**1g**), 3-FC_6H_4 (**1h**), 4-$PhOC_6H_4$ (**1i**), and 2-Naph (**1j**)) in 19−85% yields. The UV−vis spectra were rationalized in detail using time-dependent DFT and single point calculations. The fluorescence emission peaks for **1a−j** were observed at around 450 nm. Especially for **1f** and **1j**, those spectra displayed broad emission bands and relatively large Stokes shifts (3977−4503 cm^{-1}), indicating the contribution of an intramolecular charge transfer. The absolute quantum yields (0.50−0.62) of **1a−j** were higher than those of parent **8** (0.19) and 2-phenyl-1*H*-indole (0.11). The electrochemical features for **1a−j** were investigated by cyclic voltammetry. The frontier molecular orbital levels for **1a−j** were estimated based on the combination of oxidation potentials, UV−vis, and DFT calculated data. The structural property of 1,2-bis(2-phenyl-1*H*-indol-3-yl)ethyne **1a** was characterized by several spectroscopic methods and finally determined by X-ray analysis of a single crystal of **1a** recrystallized from ethyl acetate. The structural features of **1a−j** were also supported by DFT calculations.

INTRODUCTION

In recent years, molecular systems having large π-conjugations are attracting much attention due to their potential applications such as sensors,[1] organic field-effect transistors (OFETs),[2] organic light-emitting diodes (OLEDs),[3] organic solar cells (OSCs),[4] and liquid crystallines.[5] Linkage of two or more aromatic components by one or more ethynyl groups is one of the most important strategies to construct the large π-conjugated systems with various molecular architectures[6] and functions[7] because this methodology makes easy to control and tune the MO levels of the π-expanded molecular systems. For example, it was reported that oligo(phenyleneethynylene)s having electron-donating amino groups and electron-accepting diphenylboryl groups at the terminal and side positions, respectively, exhibit intense fluorescence properties in the solid state.[8] It is also known that dramatic blue and/or red shifts of emission and absorption upon coordination of metal cations occur for similar phenylene-ethynylene systems having electron donating amino groups.[9] It was also reported that

Received: November 4, 2016
Published: December 7, 2016

DOI: 10.1021/acs.joc.6b02668
J. Org. Chem. 2017, 82, 652−663

Scheme 1. Synthesis of 1,2-Bis(2-aryl-1*H*-indol-3-yl)ethynes 1a–j[a]

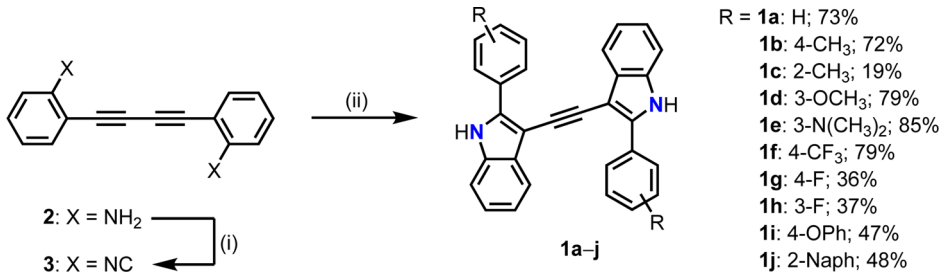

[a](i) HCO_2H (70 mol equiv)/$(CH_3CO)_2O$ (70 mol equiv), rt, 2 h; $POCl_3$, NEt_3/CH_2Cl_2 = 1/1, rt, 12 h, 80% (two steps); (ii) aryl Grignard reagent (5 mol equiv), THF, rt, 10 min.

poly(quinoline-arylene-ethynylene) copolymers exhibit intense fluorescence properties and show a significant red shift of the emission maximum from solutions to the solid state.[10] Additionally, arylene-ethynylene compounds are known to act as various types of host molecules.[11] For example, Kawase et al. found that cyclic paraphenyleneacetylene host molecules can form stable inclusion complexes with several fullerene derivatives not only in the solid states but also in solutions and studied the dynamic behavior of the complexes by temperature-variable NMR spectroscopy.[12] It is an important subject to explore new synthetic routes of acetylene-bridged π-conjugated molecules with different molecular architectures leading to the expression of novel functions.

Indole is one of the most common and ubiquitous heterocyclic frameworks incorporated in biological compounds.[13] Moreover, it has been used for the field of material sciences, which is constructed by combining with transition metals such as Ir, Ru, Re, and so on due to exhibiting luminescent features.[14] In past studies, various indole derivatives have been efficiently synthesized by transition metal-catalyzed and metal-free synthetic methods.[15] Regarding the metal-free indole synthetic methods, Youn et al. very recently synthesized substituted indoles by a metal-free C–H amination of *N*-toluenesulfonyl-2-alkenylanilines using DDQ (2,3-dichloro-5,6-dicyanobenzoquinone) as an oxidant.[16] In this new cyclization reaction, a mechanism involving a radical cation generated by a single-electron transfer and a migration process via a phenonium ion intermediate is proposed.

Regarding the synthesis of quinoline derivative by *exo*- and *endo*-ring closures of *o*-ethynylphenylisocyanides,[17] Suginome et al. first reported that isocyanide-acethylene 6-*endo*-digonal cyclization reactions with several nucleophiles such as alkoxy, amide, and malonate produce quinoline derivatives.[18] Later, Zhu and Ogawa independently found that similar reactions using tetrabutylammonium chloride as nucleophiles afford 2-chloroquinolines.[19] Although only the 6-*endo*-digonal-type cyclization reaction occurs under reported reaction conditions,[20] we found by chance that 1,2-bis(1*H*-indol-3-yl)ethyne derivatives **1** are exclusively formed by novel double 5-*exo*-digonal double cyclization reactions of 1,4-bis(2-isocyanophenyl)buta-1,3-diyne **3** as a substrate with aryl Grignard reagents. In spite of the progress of the synthetic methods for the various types of diheteroarylethyne, including the quinolone and indole derivatives, studies on the synthesis of 1,2-bis(1*H*-indol-3-yl)ethyne **8**, its derivatives,[21] and its application to functional organic materials are quite limited to the best of our knowledge. As only one exception, d'Ischia et al. synthesized 1,1′-diacetyl-3,3′-(1,2-ethynediyl)bis-5,6-diacetoxyindole by the Sonogashira coupling reaction of 1-acetyl-5,6-diacetoxy-3-ethynylindole and 1-acetyl-3-iodo-5,6-diacetoxyindole. Although UV spectra of 3,3′-(1,2-ethynediyl)bis-5,6-dihydroxyindole and its oxidized quinone tautomers were estimated by quantum chemical calculations, they did not succeed to isolate and fully characterize their deacetylated ethynylene-bridged 5,6-dihydroxyindole/5,6-indolequinone compounds due to the instability of the 5,6-dihydroxyindole system and polymerizable character of the quinonoid forms during the oxidation reaction.[22]

In this study, 1,2-bis(2-aryl-1*H*-indol-3-yl)ethyne derivatives **1a–j** having various substituents at the two aryl groups were efficiently synthesized via unusual 5-*exo*-digonal double isocyanide-acetylene cyclization reactions of 1,4-bis(2-isocyanophenyl)buta-1,3-diyne **3** and aryl Grignard reagents, and their structural, photophysical, and electrochemical properties were experimentally evaluated in detail. Additionally, structural and physicochemical features of **1a–j** were also supported by DFT calculations. Consequently, we found that the π–electron systems and orbital energy levels for 1,2-bis(1*H*-indol-3-yl)ethyne derivatives can be tuned by various aromatic substituents at 2,2′-positions of the two indole moieties.

RESULTS AND DISCUSSIONS

Synthesis of 1,2-Bis(2-aryl-1*H*-indol-3-yl)ethynes. The 1,2-bis(2-aryl-substituted-1*H*-indol-3-yl)ethyne derivatives **1a–j** were synthesized as described in Scheme 1. The compound **2** prepared from 2-ethynylaniline by dimerization using a stoichiometric amount of copper(II) acetate in pyridine/methanol under air was transformed into 1,4-bis(2-isocyanophenyl)buta-1,3-diyne **3** in 80% yield (2 steps) via a formamide intermediate. The formamide intermediate has a quite low solubility in common solvents. Before the examination of the nucleophilic cyclization of isocianide **3**, we first expected that the 6-*endo*-diagonal-type double cyclization reaction would proceed to generate the 3,3′-biquinoline analogue in accordance with previous literature.[17−19] Although we tried the cyclization reaction of **3** with various nucleophiles such as sodium amide, sodium alkoxide, and butyllithium, the attempt resulted in failure due to the formation of complex mixtures. However, in the case of using phenyl Grignard reagents as the nucleophile, we found that the 5-*exo*-digonal double cyclization process of bisisocyanide **3** exclusively occurs to produce unexpected 1,2-bis(2-phenyl-1*H*-indol-3-yl)ethyne **1a** in 79% yield. Although we do not know a clear reason, the reactions with alkyl, alkenyl, and alkynyl Grignard reagents such as ethyl, ethenyl, and phenylethynyl magnesium bromide provided the complex mixtures.

DOI: 10.1021/acs.joc.6b02668
J. Org. Chem. 2017, 82, 652–663

With respect to the adaptive range of aryl Grignard reagents, the reactions of **3** with *p*- and *o*-tolyl magnesium bromides afforded the corresponding 1,2-bis(2-tolyl-1*H*-indol-3-yl)-ethynes **1b** and **1c** in good and poor yields, respectively (**1b**: 72% and **1c**: 19%). The poor yield of **1c** should be caused by steric hindrance of the *o*-tolyl Grignard reagent as a nucleophile. Next, although we examined 4-dimethylamino-phenyl, 4-metoxyphenyl and thiophen-2-ylmagnesium bromide, the products decomposed during the purification process because the 1,2-bis(2-aryl-1*H*-indol-3-yl)ethynes having electron donating groups at 4,4′- (or 2,2′)-positions of the two aryl groups might be quite unstable to oxygen or ambient light due to their low oxidation potentials, as described below (Table 3). As an exceptional case, use of 4-phenoxyphenyl magnesium bromide provided 1,2-bis(2-(4-phenoxyphenyl)-1*H*-indol-3-yl)-ethyne **1i** in a modest yield (47%). However, 1,2-bis(2-phenyl-1*H*-indol-3-yl)ethynes with electron-donating methoxy and dimethylamino groups at the 3-positions of phenyl groups were stable under a usual purification condition (**1d**: 79% and **1e**: 85%). When 4-trifluoromethylphenyl magnesium bromide was used as a nucleophile, 1,2-bis(2-(4-(trifluoromethyl)phenyl)-1*H*-indol-3-yl)ethyne **1f** was obtained in a good yield (79%). However, the use of 4- and 3-fluorophenyl magnesium bromides resulted in a considerable decrease in yields (**1g**: 36% and **1h**: 37%). After the reaction, a considerable amount of byproduct with a low solubility was formed. Moreover, when 2-naphtylmagnesium bromide was used as a fused aromatic Grignard reagent, 1,2-bis(2-(naphthalen-2-yl)-1*H*-indol-3-yl)-ethyne **1j** was obtained in 48% yield.

The parent 1,2-di(1*H*-indol-3-yl)ethyne **8** (Chart 1) was synthesized according to a method described in the literature.[21b] All compounds were fully characterized by spectroscopic techniques such as ^{1}H and ^{13}C NMR, elemental analysis, and mass spectroscopy. Moreover, the structure of compound **1a** was identified by X-ray single crystal analysis, as discussed below (Figures 4, S48, and S49).

Chart 1. Parent 1,2-Di(1*H*-indol-3-yl)ethyne 8

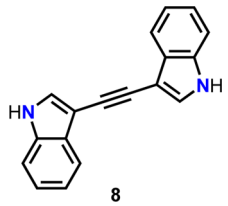

8

The plausible reaction mechanism for the formation of **1a** from 1,4-bis(2-isocyanophenyl)buta-1,3-diyne **3** with phenyl Grignard reagent is proposed in Scheme 2. First, phenyl Grignard reagents were attacked by two isocyano groups of **3** to form the dianionic phenyl adduct **4**, followed by 5-*exo*-digonal double cyclization reactions of two phenyliminomethanide moieties to generate a dianionic 3,3′-(ethyne-1,2-diyl)bis(2-phenylindol-1-ide) **5**. Among some resonance structures of **5**, the contribution of the structure where anions are located on the nitrogen atoms might be the largest. Last, the protonation of the dianionic intermediate **5** produces **1a**.

To obtain insight into the exclusive formation of 1,2-bis(2-aryl-substituted-1*H*-indol-3-yl)ethynes in these reactions, the theoretical optimizations for magnesium 3,3′-(ethyne-1,2-diyl)-bis(2-phenylindol-1-ide) dibromide **6** and magnesium (2,2′-diphenyl-3,3′-biquinolin-4-ide) dibromide **7**, which are expected as an intermediates of the cyclization reactions by the phenyl Grignard reagent as the nucleophile, were conducted at the DFT/B3LYP/6-31G(d) level (Figure S50 and Tables S1 and S2).[23] The comparison of SCF energies at the B3LYP/6-311+G(d,p) // B3LYP/6-31G(d) level for **6** and **7** revealed that the intermediate **6** is thermodynamically more stable than **7** by 17.2 kcal/mol (Figure 1). The major reason for instability of **7** should be the steric hindrance of the substituents (phenyl and MgBr) at the ortho−ortho positions of the two quinolines. On the other hand, the intermediate **6** does not have significant steric congestion, and the anion centers are located on two nitrogen atoms which possess large electron negativity in comparison with that of the carbon atom. Although the quantum calculations of the transition states from 1,4-bis(2-isocyanophenyl)buta-1,3-diyne **3** to the intermediates **6** and **7** have not succeeded so far, the preference for the 5-*exo*-digonal double cyclization can be explained by the energy difference of the two intermediate structures, as explained above.

Electronic Absorption Spectra of 1,2-Bis(2-aryl-1*H*-indol-3-yl)ethynes. To examine the electronic structures for the 1,2-bis(2-aryl-1*H*-indol-3-yl)ethyne derivatives **1a**−**j**, parent **8**, and 2-phenyl-1*H*-indole, we measured the UV−vis spectra in acetonitrile solution (1×10^{-5} M) at 298 K (Figure 2); the data are summarized in Table 1. Intriguingly, the introduction of phenyl or other aryl groups at 2,2′-positions of the two indole moieties of 1,2-bis(1*H*-indol-3-yl)ethyne induced a large and effective bathochromic shift compared to the wavelengths of the UV absorptions of parent 1,2-bis(1*H*-indol-3-yl)ethyne **8**. In fact, the absorption peaks for **1a** were observed at λ_{max}^{abs} 377 (ε = 15 700 M^{-1} cm^{-1}), 311 (ε = 26 800 M^{-1} cm^{-1}), 251 (ε = 45 900 M^{-1} cm^{-1}), and 202 nm (ε = 55 100 M^{-1} cm^{-1}) (black line in Figure 2). As discussed above, the longest λ_{max}^{abs} of **1a** showed a large bathochromic shift by 76 nm due to the introduction of phenyl groups at the 2,2′-positions of the indole moieties compared to that of **8** (301 nm, ε = 14 400 M^{-1} cm^{-1}, gray line in Figure 2). Contrary to expectations, the introduction of methyl (**1b**: blue line, 369 nm, ε = 17 400 M^{-1} cm^{-1}), fluoro (**1g**: orange line, 364 nm, ε = 21 100 M^{-1} cm^{-1}), and phenoxy groups (**1i**: red-purple line, 369 nm, ε = 18 600 M^{-1} cm^{-1}) at 4,4′-positions on the phenyl rings induced almost no red-shifts in comparison with **1a**. 2-Methylphenyl (*o*-tolyl) compound **1c** (dashed green line, 330 nm, ε = 16 000 M^{-1} cm^{-1}, as a shoulder) displayed a clear blue-shift compared to **1a** because the *o*-tolyl groups at 2,2′-positions caused a twist between the indole and tolyl groups, as discussed below (Table 4). Interestingly, we found that the 4-trifluoromethyl derivative **1f** showed a significant red-shift (red line, 386 nm, ε = 13 900 M^{-1} cm^{-1}) of longest λ_{max}^{abs}, whose terminal wavelength reached 450 nm. This spectral feature may be caused by an intramolecular charge-transfer (ICT) interaction between the electron-donating indole moieties and electron-accepting 4-trifluoromethylphenyl groups, considering that the electronic spectra for **1f** displayed a broad emission band and a large Stokes shift (vide infra). The absorption peak of 3-*N*,*N*-dimethylamino derivative (**1e**: purple line, 311 nm, ε = 26 800) shifted to a hypochromic region compared to those of 3-methoxy (**1d**: blue line, 357 nm, ε = 11 700 M^{-1} cm^{-1}) and 3-fluorophenyl derivatives (**1h**: dashed orange line, 376 nm, ε = 16 800 M^{-1} cm^{-1}), whereas the longest absorption edge wavelength of each compound was almost the same. The longest absorption peak of 2-naphthyl derivative **1j** (light green line, 379 nm, ε = 17 700 M^{-1} cm^{-1}) was observed at a relatively long wavelength region due to the extended π-conjugation,

DOI: 10.1021/acs.joc.6b02668
J. Org. Chem. 2017, 82, 652−663

Scheme 2. Plausible Reaction Mechanism of 5-*exo*-Digonal Double Cyclization of 1,4-(2-Isocyanophenyl)butadiyne 3 with Phenyl Grignard Reagent

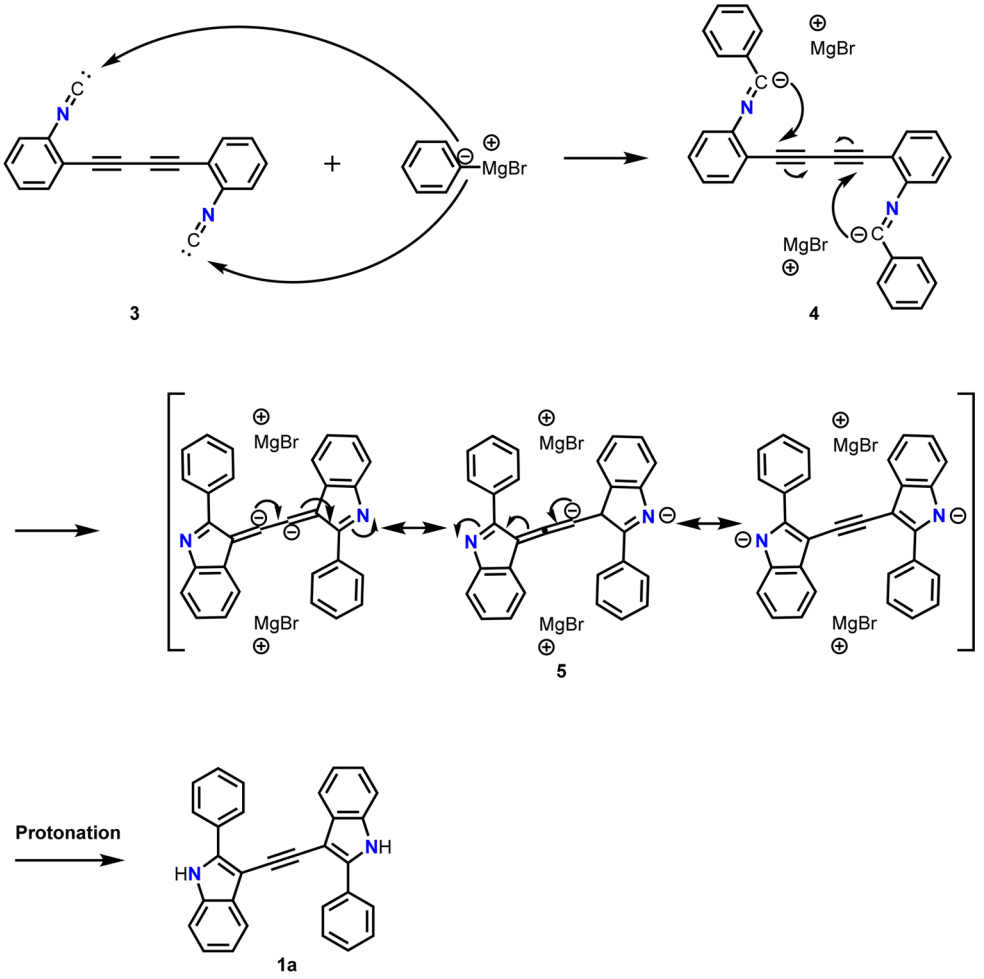

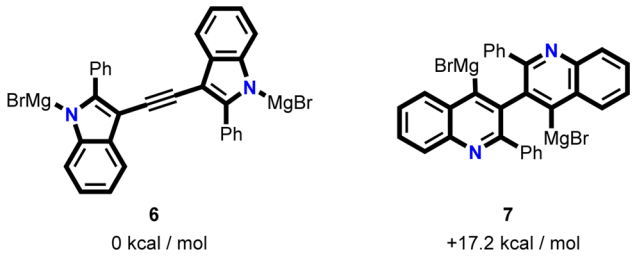

Figure 1. Energy difference between magnesium 3,3′-(ethyne-1,2-diyl)bis(2-phenylindol-1-ide) dibromide **6** and magnesium (2,2′-diphenyl-3,3′-biquinolin-4-ide) dibromide **7** at the B3LYP/6-311+G(d,p) // B3LYP/6-31G(d) level of theory.

whose absorption edge reached 450 nm. In this case, the contribution of an intramolecular charge transfer interaction is considered, as discussed below. On the other hand, interestingly, λ_{max}^{abs} and molar absorption coefficient for 1,2-bis(1*H*-indol-3-yl)ethyne **8** (gray line, 301 nm, ε = 14 400 M^{-1} cm^{-1}) were shorter and smaller than those of 2-phenyl-1*H*-indole (dashed gray line, 309 nm, ε = 20 500 M^{-1} cm^{-1}), respectively. The substitution at 2-position of indole is more effective to expand the π-conjugation than that at the 3-position from the results of both UV−vis absorption wavelengths. This result was also supported by the theoretical calculations (vide infra).

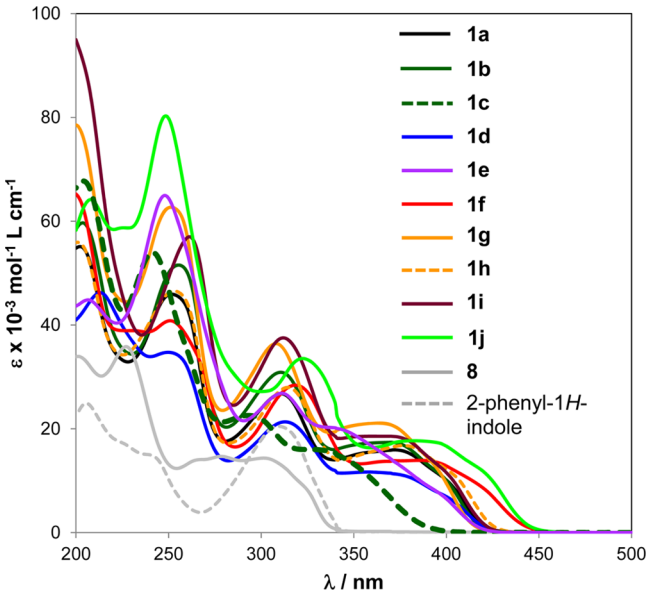

Figure 2. Electronic absorption spectra of **1a**−**j**, **8**, and 2-phenyl-1*H*-indole in CH_3CN at 298 K.

Fluorescence Spectra of 1,2-Bis(2-aryl-1*H*-indol-3-yl)-ethynes. It was confirmed that **1a**−**j** and parent **8** displayed

DOI: 10.1021/acs.joc.6b02668
J. Org. Chem. 2017, 82, 652−663

Table 1. UV−Vis Spectral Data and Calculated Lowest Absorption Maxima of 1a−j, 8, and 2-Phenyl-1*H*-indole[a,b]

compound	λ_{max}^{abs}[a]/nm (eV)	ε/M^{-1} cm^{-1}	$\lambda_{max}^{calcd\ abs}$[b]/nm ($f$)	composition of band and CI coefficients[b]
1a	202 (6.13)	55 100	412 (0.473)	H → L, 98%
	251 (4.94)	45 900		
	311 (3.99)	26 800		
	377 (3.29)	15 700		
1b	204 (6.08)	59 700	413 (0.520)	H → L, 98%
	255 (4.86)	51 500		
	311 (3.99)	30 900		
	369 (3.36)	17 400		
1c	204 (6.08)	67 700	400 (0.421)	H → L, 98%
	241 (5.15)	54 000		
	293 (4.23)	22 600		
	330[c] (3.76)	16 000		
1d	213 (5.82)	46 200	412 (0.528)	H → L, 98%
	250 (4.96)	34 700		
	313 (3.96)	21 400		
	357 (3.43)	11 700		
1e	206 (6.02)	44 800	409 (0.554)	H → L, 98%
	248 (5.00)	65 000		
	311 (3.99)	26 800		
	341[c](3.64)	20 100		
1f	251 (4.94)	40 800	439 (0.475)	H → L, 99%
	318 (3.90)	28 400		
	386 (3.21)	13 900		
	425[c] (2.92)	6900		
1g	200 (6.20)	78 600	405 (0.485)	H → L, 98%
	250 (4.96)	62 600		
	308 (4.03)	36 400		
	364 (3.41)	21 100		
1h	200 (6.20)	55 900	420 (0.468)	H → L, 98%
	253 (4.90)	46 500		
	314 (3.95)	28 000		
	376 (3.30)	16 800		
1i	261 (4.75)	57 000	413 (0.710)	H → L, 98%
	312 (3.97)	37 500		
	369 (3.36)	18 600		
1j	209 (5.93)	64 000	448 (0.639)	H → L, 99%
	248 (5.00)	80 200		
	322 (3.85)	33 500		
	379 (3.27)	17 700		
	421[c] (2.95)	11 500		
8	201 (6.17)	34 000	320 (0.405)	H → L, 94%
	227 (5.46)	35 800		
	278 (4.46)	14 700		
	301 (4.12)	14 400		
2-phenyl-1*H*-indole	206 (6.02)	24 900	304 (0.466)	H−1 → L, 2%; H → L, 98%
	240[c] (5.17)	15 000		
	309 (4.01)	20 500		

[a]Measured using CH_3CN solutions (1×10^{-5} M). [b]The data were afforded by TDDFT calculations at the B3LYP/6-31G(d) level of theory using the structures at the same level of optimization. [c]Peak as the shoulder. f = oscillator strength. H = HOMO. L = LUMO. [d]CI = configuration interaction

intense fluorescent characteristics in solutions. Figure 2 shows the normalized fluorescence spectra of **1a−j**, parent **8**, and 2-phenyl-1*H*-indole in CH_3CN (1×10^{-6} M) at 298 K, and the spectral data are summarized in Table 2. As shown in Figure 3, the wavelengths and shapes of emission peaks for **1a**, **1b**, **1d**, **1e**, **1g**, **1h**, and **1i** were almost the same (two peak tops at around 425 and 445 nm). The DFT calculation revealed that the estimated dihedral angle between the indole and aryl units (summarized in Table 4) is strongly correlated with the measured Stokes shift (ν_{ST}). For instance, 2-methyl derivative **1c** with the largest dihedral angle (44.3°, Table 4) arising from the steric hindrance between the 2-methylphenyl and indole moieties displayed the largest ν_{ST} value (7472 cm^{-1}, Table 2). In addition, 3-*N*,*N*-dimethylamino derivative **1e**, which displays a large ν_{ST} value (5796 cm^{-1}), has a relatively large indole−aryl dihedral angle (29.3°, Table 4), in agreement with a hypochromic shift of the λ_{max}^{abs} (341 nm). These results imply that the compound having a relatively large dihedral angle in ground state changes to a planate structure in the excited state.[24] On the other hand, broad fluorescent peaks were observed at 456 and 457 nm for 4-trifluoromethyl derivative **1f** (red line) and 2-naphtyl derivative **1j** (lime green), respectively. The presence of ICT interaction is estimated from the fact that **1f** and **1j** showed broad emission bands, relatively large ν_{ST} values, and average dihedral angles (Table 4).

As shown in Table 2, we determined the absolute fluorescence quantum yields (Φ_f) by an integrating sphere system. Compounds **1a−1j** showed moderate to somewhat high Φ_f values (0.50−0.62) regardless of the kind of substituents, whereas the values of parent **8** and 2-phenylindole (0.19 and 0.11, respectively) were low. Although we do not know a clear reason, 4-fluoro and 4-phenoxy derivatives **1g** and **1i** showed the highest Φ_f value (0.62 each) among all compounds **1a−j**. The introduction of aryl groups to 2,2′-positions of the indole moieties of parent **8** caused the increase in ε and Φ_f values of the emitter.

The fluorescence efficiency is determined by the balance between radiative and nonradiative decay constants. In this study, there was little difference in fluorescence quantum yields of all compounds **1a−j**, as discussed above. To elucidate the reason and gain further insight into the photophysical properties for **1a−j**, we examined the fluorescence lifetime (τ_f) and calculated radiative (k_{rd}) and nonradiative decay rate constants (k_{nr}) based on the equations $k_{rd} = \Phi_f/\tau_f$ and $k_{nr} = (1 - \Phi_f)/\tau_f$. The 4-trifluoromethyl derivative **1f** and 2-naphthyl derivative **1j** exhibited relatively large τ_f values (3.200 and 3.088 ns), as summarized in Table 2. These results imply that the charge separation between the electron-donating indole moiety and electron-deficient 4-trifluoromethylphenyl or 2-naphthylphenyl group occurred to some extent in the excited state of **1f** or **1j**, consistent with the results of ICT interaction, as shown above. The τ_f values (2.540−2.704 ns) of other compounds, **1a−e** and **1g−i** were shorter than those (3.088−3.200 ns) of **1f**, **1j**, **8** and 2-phenylindole.

Although there was no clear correlation between the calculated rate constants (k_{rd} and k_{nr}) and the type of substituents, a certain degree of correlation was observed between k_{rd}/k_{nr} and Φ_f (Table 2). Although 4-phenoxy derivative **1i** displayed the highest k_{rd} (24.1×10^7 s^{-1}), the k_{nr} was relatively small (14.8×10^7 s^{-1}). Thus, the highest Φ_f value (0.62) of **1i** is attributable to the fast radiative and relatively slow nonradiative processes. Also, 4-fluoro derivative **1g**, having the second highest k_{rd} (22.9×10^7 s^{-1}) and lowest k_{nr} (14.1×10^7 s^{-1}), displayed the highest Φ_f value (0.62). On the other hand, 2-phenyl-1*H*-indole and parent **8**, with the lowest and second lowest k_{rd} values (3.56×10^7 and 6.02×10^7 s^{-1}, respectively) and the largest and second largest k_{nr} values (28.8×10^7 and 25.7×10^7 s^{-1}, respectively) displayed the

DOI: 10.1021/acs.joc.6b02668
J. Org. Chem. 2017, 82, 652−663

Table 2. Fluorescence Data of 1a–1j, 8, and 2-Phenyl-1*H*-indole[a]

compound	λ_{max}^{abs}/nm (in CH_3CN)	λ_{ex}/nm	λ_{max}^{fl}/nm (in CH_3CN)	ν_{ST}/cm^{-1}[b] (in CH_3CN)	Φ_f[c]	τ_f[d]/ns	k_{rd}[e]/10^7 s^{-1}	k_{nr}[f]/10^7 s^{-1}
1a	377	375	424 447	2940	0.55	2.707	20.3	16.6
1b	369	370	421 446	3347	0.58	2.629	22.1	16.0
1c	330	330	438	7472	0.53	2.959	17.9	15.9
1d	357	355	425 452	4482	0.59	2.666	22.1	15.4
1e	341	340	425 443	5796	0.50	2.540	19.7	19.7
1f	386	385	456 469[c]	3977	0.53	3.200	16.6	14.7
1g	364	365	419 442	3606	0.62	2.704	22.9	14.1
1h	376	375	430 453	3340	0.57	2.688	21.2	16.0
1i	369	370	426 449	3626	0.62	2.569	24.1	14.8
1j	379	380	457 474[c]	4503	0.55	3.088	17.8	14.6
8	301	300	369	6122	0.19	3.156	6.02	25.7
2-phenyl-1*H*-indole	309	310	362	4738	0.11	3.088	3.56	28.8

[a]Measured using CH_3CN solutions (1×10^{-6} M). Excited at each λ_{max}^{abs}. [b]Stokes shift. [c]Absolute quantum yields determined by an integrating sphere system. [d]Fluorescence lifetime. [e]Radiative decay rate constant. [f]Nonradiative decay rate constant.

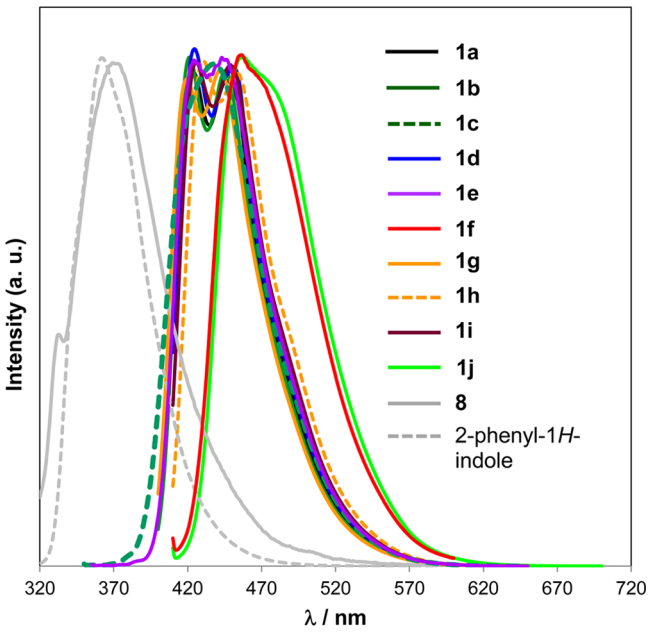

Figure 3. Normalized fluorescence spectra of **1a–1j**, **8**, and 2-phenyl-1*H*-indole in CH_3CN at 298 K.

lowest and second lowest Φ_f values (0.19 and 0.11, respectively).

Electrochemistry of 1,2-Bis(2-aryl-1*H*-indol-3-yl)-ethynes. Electrochemical properties for **1a–j**, **8**, and 2-phenyl-1*H*-indole were also investigated by cyclic voltammetry in dichloromethane containing 0.1 mol L^{-1} *n*-Bu_4NPF_6 as a supporting electrolyte (Figures S35–S46). Table 3 summarizes the experimentally measured oxidation (anodic) peak potential (E_{pa}), oxidation onset potential (E_{onset}) versus Fc^+/Fc (ferrocenium/ferrocene couple), energy levels of the highest occupied molecular orbital (HOMO), lowest unoccupied molecular orbital (LUMO), and their gap ($\Delta E_{HOMO-LUMO}$) calculated at the B3LYP/6-311+G(d,p) // B3LYP/6-31G(d) level in addition to the optical HOMO–LUMO gap (ΔE_{opt}) for all compounds.

1,2-Bis(2-aryl-substituted-1*H*-indol-3-yl)ethynes **1a–j** exhibited irreversible first oxidation potentials between 0.16 and 0.39 V, indicating that the generated radical cation species are very unstable. The E_{pa} and E_{onset} (0.26 and 0.097 V, respectively) for **1a** were lower than those (0.32 and 0.19 V, respectively) of parent **8**, indicating that the introduction of phenyl groups at 2,2′-positions of the indole moieties caused the HOMO level to rise due to the efficient elongation of π-conjugation between the bisindolylethyne framework and phenyl groups. The extension of π-conjugation for **1a** is also supported by the fact that $\Delta E_{HOMO-LUMO}$ (3.32 eV) and ΔE_{opt} (3.29 eV) of **1a** are smaller than those of parent **8** (4.12 and 4.12 eV) (Table 3). The E_{pa} and E_{onset} (0.20 and 0.074 V, respectively) of *p*-tolyl compound **1b** were lower than those of **1a**. However, those of *o*-tolyl compound **1c** (0.31 and 0.14 V) were significantly higher than those of **1b**. This result is consistent with the fact that the HOMO level of **1c** is slightly lower than that of **1b**, indicating that the π-conjugation between bisindolylethyne and 2-tolyl group for **1c** is disturbed by the steric hindrance. Although the E_{pa} and HOMO level of 3-methoxyphenyl compound **1d** were almost the same as those of **1a**, those of 3-dimethylaminophenyl compound **1e** were lower and higher than those of **1a**, respectively, reflecting that the dimethylamino group is a stronger electron-donating group than the methoxy group. On the other hand, 4-trifluoromethylphenyl compound **1f** exhibited the highest E_{pa} and lowest HOMO level among **1a–j**, attributable to a strong inductive electron-withdrawing effect of the trifluoromethyl groups. Although there was not a large difference in HOMO levels and E_{onset} values between 4-fluoro and 3-fluoro derivatives **1g** and **1h**, the LUMO level (−1.80 eV) of 4-fluoro derivative **1g** was higher than that (−1.93 eV) of 3-fluoro derivative **1h**,

DOI: 10.1021/acs.joc.6b02668
J. Org. Chem. 2017, 82, 652–663

Table 3. Electrochemical Data of 1a–j, 8, and 2-Phenyl-1*H*-indole in CH_2Cl_2 (0.1 mol L^{-1} *n*-Bu_4NPF_6);[a] Theoretically Calculated FMO Levels and Gaps ($\Delta E_{HOMO-LUMO}$);[b] and Optical HOMO–LUMO Gaps (ΔE_{opt})[c]

compond	E_{pa}/V	E_{onset}/V	HOMO[b,d]/eV	LUMO[b]/eV	$\Delta E_{HOMO-LUMO}$[b]/eV	ΔE_{opt}[c]/eV
1a	0.26[e]	0.097	−5.03 (−4.90)	−1.71	3.32	3.29
1b	0.20[e]	0.074	−4.93 (−4.87)	−1.60	3.33	3.36
1c	0.31[e]	0.14	−4.96 (−4.94)	−1.49	3.47	3.76
1d	0.25[e]	0.12	−4.96 (−4.92)	−1.63	3.33	3.47
1e	0.16[e]	−0.020	−4.78 (−4.78)	−1.43	3.35	3.64
1f	0.39[e]	0.25	−5.44 (−5.05)	−2.28	3.16	3.21
1g	0.28[e]	0.16	−5.17 (−4.96)	−1.80	3.37	3.41
1h	0.33[e]	0.17	−5.17 (−4.97)	−1.93	3.24	3.30
1i	0.21[e]	0.064	−4.96 (−4.86)	−1.63	3.33	3.36
1j	0.23[e]	0.11	−5.05 (−4.91)	−1.96	3.09	3.27
8	0.32[e]	0.19	−5.09 (−4.99)	−0.973	4.12	4.12
2-phenyl-1*H*-indole	0.60[e]	0.39	−5.63 (−5.44)	−1.37	5.26	4.01

[a]All potentials are given versus the Fc^+/Fc couple used as the external standard; scan rate = 100 mV s^{-1}. [b]Calculated by B3LYP/6-311+G(d,p) // B3LYP/6-31G(d) for **1a–j**, **8**, and 2-phenyl-1*H*-indole. [c]The values are calculated from the longest λ_{max}^{abs}. [d]The values in the parentheses are those deduced from the inset values according to the following equation: HOMO = −(4.8 + E_{onset}) eV (ref 25). [e]Irreversible wave.

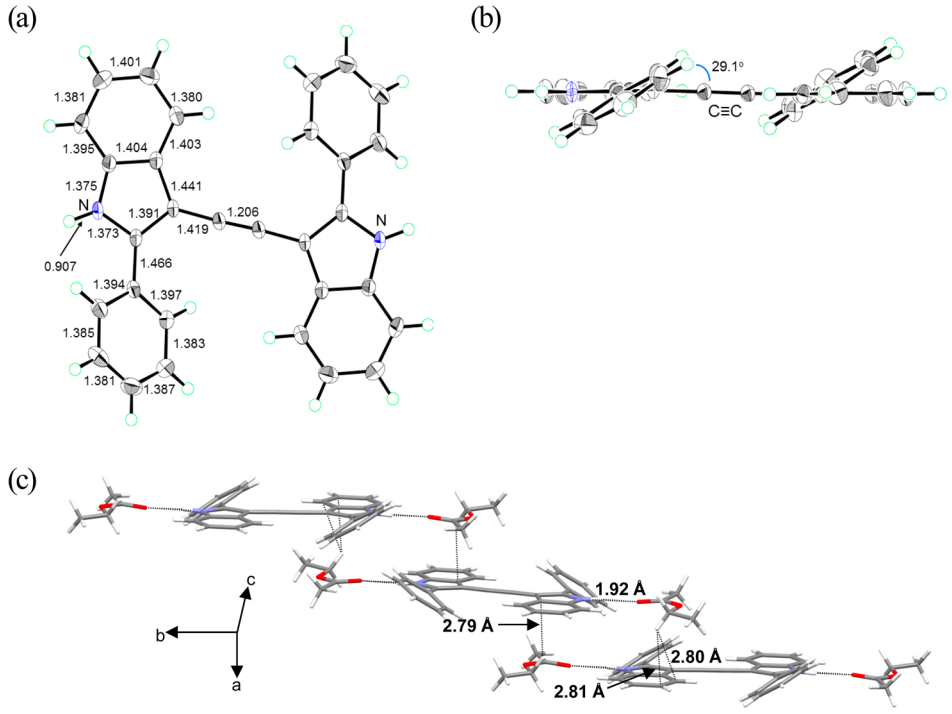

Figure 4. X-ray crystal structure of 1,2-bis(2-phenyl-1*H*-indol-3-yl)ethyne **1a** at 173 K. (a) Top view. The values are each bond length. (b) Side view. The value is the tilt angle of the phenyl ring. The atoms are drawn as 50% probability ellipsoids. Solvent molecule is omitted for clarity. (c) Packing diagram of **1a**. Dashed lines are within the sum of the van der Waals radius. The values are lengths of molecular interaction.

which is attributable to a stronger electron-donating effect of 4-fluorophenyl group by resonance than that of 3-fluorophenyl group. As a result, the $\Delta E_{HOMO-LUMO}$ and ΔE_{opt} of **1g** were higher than those of **1h**. The oxidation potentials and $\Delta E_{HOMO-LUMO}$ of 4-phenoxy derivative **1i** were almost the same as those of **1a**. Although the E_{pa}, E_{onset}, and HOMO level of naphthyl derivative **1j** were almost the same as those of **1a**, the former LUMO level was lower than the latter one, that is, the former $\Delta E_{HOMO-LUMO}$ is lower than the latter one. This result should be attributed to the sp^2 inductive effect of the naphthyl groups of **1j**.

The results discussed above suggested that the introduction of aryl groups at 2,2′-positions of the indole moieties of parent **8** caused the HOMO–LUMO gap to reduce as a consequence of a lowering of the LUMO level and small change of the HOMO level for the 1,2-bis(1*H*-indol-3-yl)ethyne derivatives. For example, the difference of $\Delta E_{HOMO-LUMO}$ between phenyl-substituted **1a** and parent **8** is 0.80 eV; as a consequence, the differences of the HOMO levels and LUMO levels are 0.06 and 0.737, respectively (Table 2). The trend of the $\Delta E_{HOMO-LUMO}$ for 1,2-bis(2-aryl-substituted-1*H*-indol-3-yl)ethynes **1a–j** was almost identical to that of the ΔE_{opt} calculated from the observed longest λ_{max}^{abs}. On the other hand, the E_{pa} and HOMO levels (0.60 V and −5.63 eV) of 2-phenyl-1*H*-indole are higher and lower than those (0.26 V and −5.03 eV) of **8**, respectively. However, the ΔE_{opt} of 2-phenyl-1*H*-indole is almost the same as that of **8** due to a lowering of the LUMO level (Table 2).

X-ray Crystal Structure of 1a. The structure of 1,2-bis(2-phenyl-1*H*-indol-3-yl)ethyne **1a** was confirmed and analyzed by

DOI: 10.1021/acs.joc.6b02668
J. Org. Chem. 2017, 82, 652–663

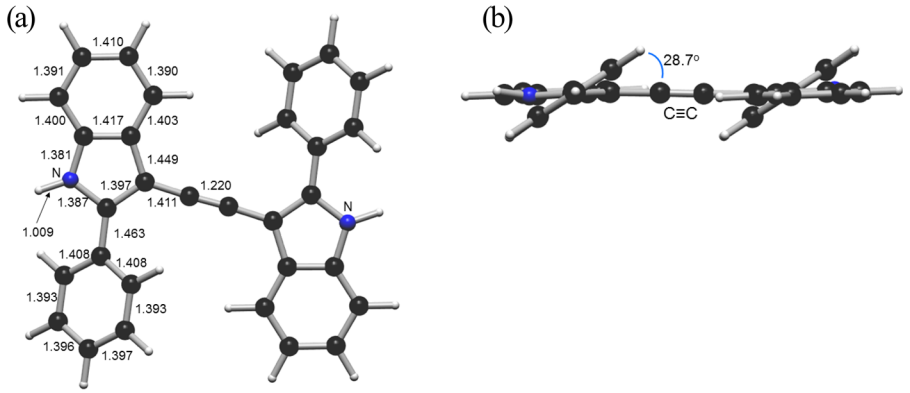

Figure 5. DFT optimized structure of **1a** at the B3LYP/6-31G(d) level. The values are each bond length. (a) Top view. (b) Side view.

an X-ray crystallographic analysis of its single crystal, which was obtained by recrystallization using ethyl acetate (Figures 4, S48, and S49). The single crystal was a clathrate consisting of **1a** and ethyl acetate with a 1:1 stoichiometry. The two indole moieties jointed by the ethynyl linker for **1a** are coplanar, and the two phenyl groups at 2,2′-positions are tilted by 29.1° with respect to each indole ring. The C≡C bond length of **1a** is 1.206 Å, which is almost the same as a typical acetylenic bond length (1.21 Å). The clathrate, which was formed by the hydrogen bond (1.92 Å) between the indolyl-H of **1a** and carbonyl moiety of ethyl acetate, is matched in a one-dimentional continuous structure along the *b*-axis, as is shown in Figure 4c. The one-dimensional continuous structure with attractive short contacts of 2.788−2.806 Å is formed by CH−π interactions between CH_2 of the ethyl acetate and some sp^2 carbons of one indole ring of **1a**.

Theoretical Calculations of 1,2-Bis(2-aryl-1*H*-indol-3-yl)ethynes. To gain further structural insight, we optimized the ground state structure of 1,2-bis(2-phenyl-1*H*-indol-3-yl)ethyne **1a** by means of DFT calculation at the B3LYP/6-31G(d) level (Figure 5), and compared the results with the X-ray molecular structure of **1a**. The calculated dihedral angle of indole-ethynyl-indole and C≡C bond length of **1a** are 0 and 1.22° Å, respectively (Figure 5a). Moreover, the phenyl group of the calculated **1a** was twisted by 28.7° from the indole-ethynyl-indole plane (Figure 5b). The calculated angle is slightly smaller by 0.4° than that evaluated from the X-ray crystal structure. The theoretical data correspond reasonably well with the experimental data, suggesting that the X-ray structural features of **1a** in the solid state are intrinsic and not affected by packing effects. The other calculated structural details and MO features for **1a**−**j**, **8**, and 2-phenyl-1*H*-indole at the same level are discussed below.

The calculated structures for **1a**−**j**, **8**, and 2-phenyl-1*H*-indole (see also Figures S51−S62) and their structural details are summarized in Table 4. In a manner similar to that of **1a**, the dihedral angles between the indole and aryl ring optimized by B3LYP/6-31G(d) level of theory were 25−29° for **1b**−**j** except *o*-tolyl compound **1c**. The dihedral angle (44°) for **1c** was much larger than that of the other derivatives owing to the steric hindrance. Next, dihedral angles between two indole moieties jointed by the acetylene bridge were 0° for **1a**−**e** and **8** and 12−14° for **1f**−**j** (Table 4). The relatively large torsions for **1f**−**j** did not have much influence for their electronic spectra. This result is supported by the fact that the rotational barrier for the acetylene axis of diarylethynes is generally low.[26] On the other hand, the large dihedral angle between the indole and aryl group had a great influence on the fluorescence property and Stokes shift, as discussed above.

Table 4. Structural Data of Compounds 1a−j, 8, and 2-Phenyl-1*H*-indole[a]

compound	dihedral angle (indole-phenyl)/deg	dihedral angle (indole- indole)/deg
1a	28.7 (29.1)	0 (0)
1b	28.5	0
1c	44.3	0
1d	28.0	0
1e	29.3	0
1f	25.5	13.2
1g	26.4	14.0
1h	25.8	14.1
1i	25.9	12.3
1j	25.0	13.2
8		0
2-phenyl-1*H*-indole	24.9	

[a]Calculations were performed at B3LYP/6-31G(d) level of theory. Measured values by X-ray crystal analysis for **1a** are in parentheses.

The time-dependent (TD) DFT and single point calculations using global minimum optimized structures for compounds **1a**−**j**, **8**, and 2-phenyl-1*H*-indole were performed to analyze the correlation between their structural and electronic properties. The results of TDDFT calculations are summarized in Table 1. The calculations revealed that the HOMO−LUMO transitions mainly contribute to λ_{max}^{abs} values for **1a**−**j** and **8**, whereas the HOMO−1 to LUMO transition in addition to the HOMO−LUMO transition is related to λ_{max}^{abs} for 2-phenyl-1*H*-indole. The calculated λ_{max}^{abs} values (400−448 nm) were relatively shorter by 35−70 nm than the λ_{max}^{abs} values evaluated from the measured spectra of all the compounds except for 2-phenyl-1*H*-indole in acetonitrile because the calculations were carried out in the gas-phase conditions. However, the trend of calculated absorption wavelength was in accordance with those of the measured absorption wavelength. For instance, the calculated λ_{max}^{abs} of parent **8** (320 nm, f = 0.405) was shorter by 92 nm than that of diphenyl-substituted **1a** (412 nm, f = 0.473). This difference (92 nm) between **1a** and **8** was comparable to the difference (76 nm) of measured λ_{max}^{abs} between **1a** and **8**. In addition, the calculated λ_{max}^{abs} values of **1a** and 2-methyl derivative **1b** (412 and 413 nm, f = 0.473 and 0.520, respectively) were almost the same wavelength as each other, in agreement with the fact that the observed λ_{max}^{abs} of **1a** (377 nm) is comparable to that of **1b** (369 nm). The calculated

DOI: 10.1021/acs.joc.6b02668
J. Org. Chem. 2017, 82, 652−663

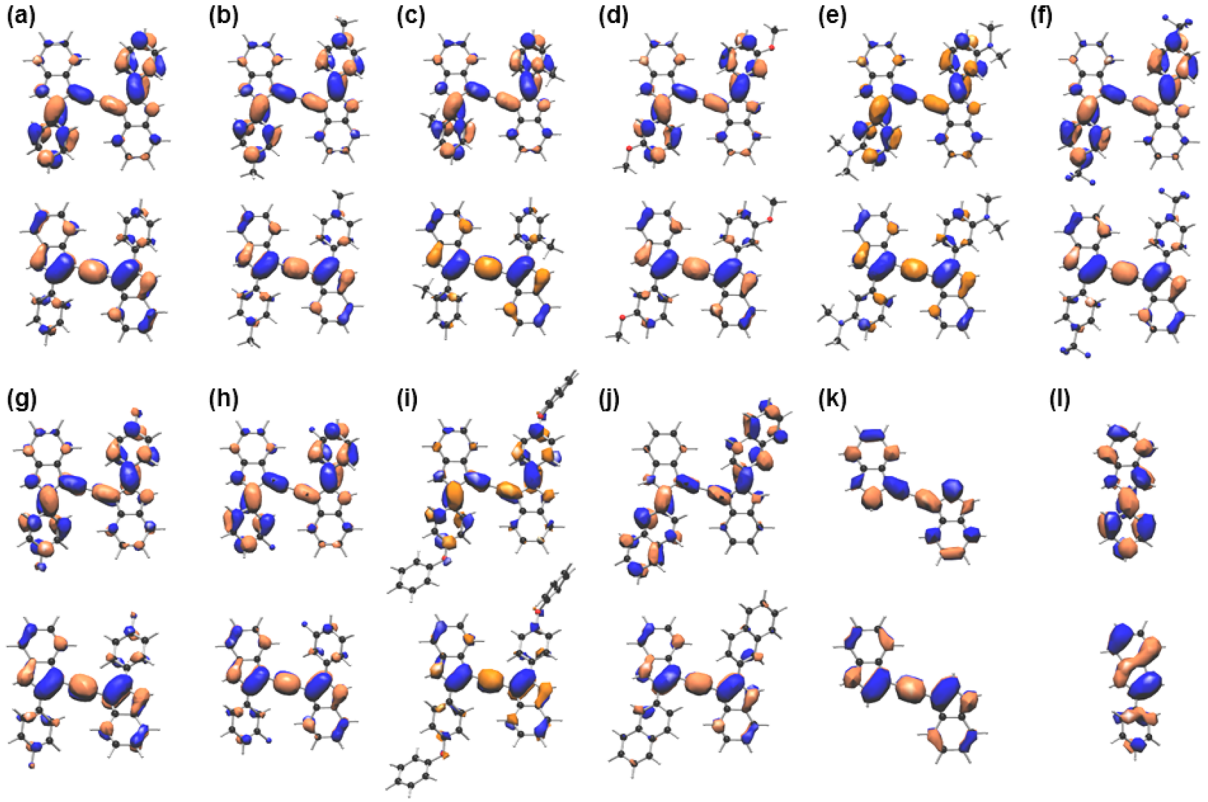

Figure 6. Calculated FMO orbitals (RB3LYP/6-311+G(d,p) // RB3LYP/6-31G(d)) of (a) **1a**, (b) **1b**, (c) **1c**, (d) **1d**, (e) **1e**, (f) **1f**, (g) **1g**, (h) **1h**, (i) **1i**, (j) **1j**, (k) **8**, and (l) 2-phenyl-1*H*-indole. HOMOs and LUMOs are shown at the bottom and top, respectively.

λ_{max}^{abs} of 4-trifluoromethyl derivative **1f** was 439 nm (f = 0.475), which was longer by 27 nm than that of **1a**. This large red-shift is attributed to the ICT interaction, as described above. A similar ICT interaction is estimated for 2-naphthyl derivative **1j**, whose calculated λ_{max}^{abs} is 448 nm with a relatively large oscillator strength (f = 0.639) (Table 1).

We carried out the single point calculation to investigate the electronic effects of various substituents on the 1,2-di(1*H*-indol-3-yl)ethyne. Figure 6 shows calculated structures and FMO plots at the RB3LYP/6-311+G(d,p) // RB3LYP/6-31G(d) level of theory. The HOMO orbital for **1a**−**j** is almost confined on the two indole moieties and acetylene bridge, whereas the electronic effects of the aryl substituents on HOMO are very weak. On the other hand, the LUMO for **1a**−**j** is mainly localized on both the aryl group and ethynylene spacer, where nodal planes are present. Furthermore, the calculation revealed that both the HOMO and LUMO for **8** and 2-pheny-1*H*-lindole spread all over the molecule. It is noted that the LUMO orbital densities of **1f** and **1j** are located on the substituents (CF_3 for **1f** and 2-naphthyl for **1j**), supporting the presence of ICT interactions (Figures 6f and j).

Again, although there are some differences in numerical values between experimental and theoretical absorption spectra, trends in relative change of the observed λ_{max}^{abs} for 1,2-bis(2-aryl-1*H*-indol-3-yl)ethyne **1a**−**j**, **8**, and 2-phenyl-1*H*-indole were reproduced well by TDDFT and single point calculations.

CONCLUSIONS

In summary, we synthesized a series of 1,2-bis(2-aryl-1*H*-indol-3-yl)ethynes **1a**−**j** via the double isocyanide-acetylene cyclization reactions of 1,4-bis(2-isocyanophenyl)buta-1,3-diyne **3** using aryl Grignard reagents as a nucleophile. The adaptive range of aryl Grignard reagents was found to be wide under this reaction condition because various aryl Grignard reagents such as C_6H_5, 4-$H_3CC_6H_4$, 2-$H_3CC_6H_4$, 3-$MeOC_6H_4$, 3-$(CH_3)_2NC_6H_4$, 4-$F_3CC_6H_4$, 4-FC_6H_4, 3-FC_6H_4, 4-$PhOC_6H_4$, and 2-Naph can be used. UV−vis spectra of **1a**−**j** revealed that the π-connectivity of these compounds increased by the substitution of aryl groups at 2,2′-positions of the two indole moieties. The π-conjugation expansions for **1a**−**j** compared to those of aryl-unsubstituted **8** were also rationalized by the oxidation potentials and their HOMO−LUMO gaps calculated from MO calculation. The fluorescence spectral analysis revealed that there is an intramolecular charge-transfer interaction between the aryl and indole moieties for 4-$CF_3C_6H_4$ and 2-naphthyl derivatives, which is supported by the large ν_{ST} values and broad emission bands. Moreover, we found that the ν_{ST} value is largely affected by the dihedral angle between indole and aryl moieties. The absolute fluorescence quantum yields for **1a**−**j** were much higher than those of parent **8** and 2-pheny-1*H*-lindole. The reason for this can be found in the fact that the radiative pass for **1a**−**j** is faster than those for parent **8** and 2-phenylindole, and inversely, the nonradiative pass for the latter is faster than that for the former. Furthermore, characteristics of the molecular structure and absorption spectra derived from the experiments for **1a**−**j** were successfully reproduced by DFT calculations. Actually, there was a good agreement between the X-ray crystal structure and DFT-optimized structure for **1a**. The HOMO energy levels and $\Delta E_{HOMO-LUMO}$ values calculated based on the optimized structures at the same level of theory were almost consistent with the measured HOMO energy levels and ΔE_{opt} values. 1,2-Bis(2-aryl-1*H*-indol-3-yl)ethynes are promising electron-donating materials whose orbital levels are easily controllable by

DOI: 10.1021/acs.joc.6b02668
J. Org. Chem. 2017, 82, 652−663

changing the substituents on the aryl groups. Further studies on diindolylethyne-based π-conjugated functional molecules utilizing the isocyanide-acetylene cyclization are in progress in our laboratory.

EXPERIMENTAL SECTION

General Experimental Methods. All chemicals and solvents were purchased from commercial sources and were used without further purification unless stated otherwise. Column chromatography and plug filtrations were carried out with SiO_2 60. Thin-layer chromatography (TLC) was conducted on aluminum sheets coated with SiO_2 60 F 254; visualization was done with a lamp (254 or 365 nm). Melting points (mp) are uncorrected. IR spectra were measured as KBr pellets or neat on NaCl disks. UV−vis spectra were recorded in a 10 mm width quartz cell. The UV−vis and fluorescence spectra were measured in a cuvette of 1 cm at 298 K. The absorption maxima (λ_{max}^{abs}) are reported in nm with the relative intensity or the molar absorption coefficient in brackets. Shoulders are indicated as sh. Absolute quantum yields were determined by a calibrated integrating sphere system in CH_3CN. The fluorescence lifetimes were measured on a Spectra-Physics time-resolved spectrofluorometer system with a Ti:sapphire laser. CH_3CN (for the spectral measurement) was deaerated under ultrasound irradiation for 10 min just before use. ^1H NMR spectra were determined in $CDCl_3$, DMSO d_6, and acetone d_6 solvents. Chemical shifts (δ) are given as δ values (ppm) relative to tetramethylsilane (TMS). The coupling constants (J) are given in hertz. The apparent resonance multiplicity is described as s (singlet), d (doublet), t (triplet), and m (multiplet). High-resolution mass spectra (HRMS) in acetonitrile were recorded by ESI-TOF mass spectrometers. Gel-permeation chromatography was performed with $CHCl_3$. Cyclic voltammetry was performed using a cell equipped with a platinum as working electrode, a platinum wire as counter electrode, and $Ag/AgNO_3$ as the referential electrode. All electrochemical measurements were performed in the CH_2Cl_2 solution (ca. 5×10^{-4} mol L^{-1}) containing 0.1 mol L^{-1} n-Bu_4NPF_6 at 298 K. All potentials are referenced to the ferrocenium/ferrocene (Fc^+/Fc) couple, used as a standard.

*2,2′-(Buta-1,3-diyne-1,4-diyl)dianiline (**2**).* 2,2′-(Buta-1,3-diyne-1,4-diyl)dianiline (**2**) was prepared from 2-ethynylaniline according to the reported manner by Fang and Chou.[27] All spectral data were completely identical with the reported data.

*Preparation of 1,4-Bis(2-isocyanophenyl)buta-1,3-diyne (**3**).* *N*,*N*′-(Buta-1,3-diyne-1,4-diylbis(2,1-phenylene))diformamide as the precursor of 1,4-bis(2-isocyanophenyl)buta-1,3-diyne (**3**) was prepared according to following literature procedure.[28] The obtained *N*,*N*′-(buta-1,3-diyne-1,4-diylbis(2,1-phenylene))diformamide was washed with H_2O and $CHCl_3$ several times and used for the next step without further purification because the solubility of this compound into the common solvents is quite low.

N,*N*′-(Buta-1,3-diyne-1,4-diylbis(2,1-phenylene))diformamide (100.0 mg, 0.347 mmol) was dispersed into a solution of Et_3N (2 mL) and CH_2Cl_2 (20 mL). After $POCl_3$ (106.4 mg, 0.694 mmol) was dropped slowly to the slurry at ambient temperature, the mixture was stirred for 12 h, and then volatile materials were removed under reduced pressure. The residual material was purified by column chromatography on Florisil (hexane/EtOAc = 4/1 as an eluent) to give 1,4-bis(2-isocyanophenyl)buta-1,3-diyne **3** as a white solid. The obtained **3** was used for the next step quickly due to its instability. Yield, 70.0 mg (0.278 mmol), 80% (two steps); mp, 167.0−168.0 °C (decomp.); ^1H NMR (400 MHz, $CDCl_3$) δ 7.42−7.46 (6H, s), 7.67 (2H, d, J = 7.2 Hz); ^{13}C NMR (100 MHz, $CDCl_3$) δ 76.5, 78.2, 118.3, 125.2 (2C), 127.4, 128.5, 132.0, 167.2; IR (NaCl, cm^{-1} $\tilde{\nu}$ = 756, 1099, 1260, 1441, 1477, 2127, 2361; MS (LC-ESI-TOF, positive) m/z calcd for $C_{18}H_8N_2$: 252.0688 $[M]^+$; found: 252.0720.

*Typical Synthetic Procedure for 1,2-Bis(2-aryl-substituted-1H-indol-3-yl)ethynes (**1**).* All of the 1,2-bis(2-aryl-1*H*-indol-3-yl)ethyne derivatives **1a**−**j** were synthesized according to the following procedure: Into a mixture of magnesium turnings (122.7 mg, 5.1 mmol) in THF (3 mL) was added aryl bromide (5.1 mmol) in THF (5 mL) in a 20 mL Schlenk flask. The mixture was heated under N_2 atmosphere for 30 min, and then the gray slurry was cooled to room temperature. A solution of 1,4-bis(2-isocyanophenyl)buta-1,3-diyne **3** (262.4 mg, 1.04 mmol) in THF was quickly added to the aryl Grignard reagent, and the solution was stirred for 10 min at ambient temperature. After the reaction proceeding was checked by TLC, the reaction mixture was quenched with a saturated aqueous NH_4Cl solution (3 mL). After the volatile materials were removed, the residual mixture was diluted with EtOAc (20 mL) and washed with H_2O several times. The organic layer was dried over Na_2SO_4 and concentrated under reduced pressure. The residual mixture was purified by column chromatography on silica gel (hexane/EtOAc as an eluent) to give the 1,2-bis(2-aryl-1*H*-indol-3-yl)ethyne as a yellow powder. Further purification for the analysis was carried out by recycling GPC ($CHCl_3$ as an eluent) and/or reprecipitation in CH_2Cl_2 or acetone/hexane.

*1,2-Bis(2-phenyl-1H-indol-3-yl)ethyne (**1a**).* Yield, 310.1 mg (73%); R_f = 0.30 (hexane/EtOAc = 5/1); mp, 231.5−232.5 °C; ^1H NMR (400 MHz, $CDCl_3$) δ 7.22−7.30 (4H, m), 7.37−7.42 (4H, m), 7.47 (4H, t, J = 7.2 Hz), 7.91 (2H, d, J = 7.2 Hz), 8.15 (4H, d, J = 7.6 Hz), 8.35 (2H, br-s); ^{13}C NMR (100 MHz, $CDCl_3$) δ 87.9, 97.3, 111.0, 120.3, 120.9, 123.5, 126.5, 128.3, 128.9, 130.6, 131.9, 135.5, 138.6; IR (KBr, cm^{-1}) $\tilde{\nu}$ = 690, 737, 1238, 1327, 1454, 1504, 3421; UV (CH_3CN, nm) 202, 251, 311, 377; FL (CH_3CN, nm) 424, 447; elemental analysis calcd (%) for $C_{30}H_{20}N_2 \cdot 0.05CHCl_3$: C, 87.08; H, 4.88; N, 6.76%; found: C, 87.08; H, 4.88; N, 6.83%; MS (LC-ESI-TOF, positive) m/z calcd for $C_{30}H_{20}N_2$: 408.1627 $[M]^+$; found: 408.1650.

*1,2-Bis(2-(p-tolyl)-1H-indol-3-yl)ethyne (**1b**).* Yield, 327.0 mg (72%); R_f = 0.30 (hexane/EtOAc = 5/1); mp, 230.5−231.5 °C; ^1H NMR (400 MHz, DMSO d_6) δ 2.42 (6H, s), 7.19−7.25 (4H, m), 7.34 (4H, d, J = 7.6 Hz), 7.48 (2H, d, J = 7.6 Hz), 7.88 (2H, d, J = 7.2 Hz), 8.25 (4H, d, J = 8.0 Hz), 10.8 (2H, br-s); ^{13}C NMR (100 MHz, DMSO d_6) δ 30.8, 88.4, 94.7, 111.9, 118.9, 120.5, 122.9, 126.4, 129.0, 129.4, 129.9, 135.8, 137.9, 138.7; IR (KBr, cm^{-1}) $\tilde{\nu}$ = 737, 814, 1234, 1458, 1512, 3391; UV (CH_3CN, nm) 204, 255, 311, 369; FL (CH_3CN, nm) 421, 446; elemental analysis calcd (%) for $C_{32}H_{24}N_2 \cdot 0.05CHCl_3$: C, 87.08; H, 4.88; N, 6.76%; found: C, 86.59; H, 5.67; N, 6.31%; MS (LC-ESI-TOF, positive) m/z calcd for $C_{32}H_{24}N_2$: 436.1940 $[M]^+$; found: 436.1914.

*1,2-Bis(2-(o-tolyl)-1H-indol-3-yl)ethyne (**1c**).* Yield, 86.3 mg (19%); R_f = 0.30 (hexane/EtOAc = 6/1); mp, 213.5−214.5 °C; ^1H NMR (400 MHz, $CDCl_3$) δ 2.38 (6H, s), 7.17−7.37 (12H, m), 7.54 (2H, d, J = 7.6 Hz), 7.48 (2H, d, J = 7.6 Hz), 7.69 (2H, d, J = 7.6 Hz), 8.25 (4H, d, J = 8.0 Hz), 8.06 (2H, br-s); ^{13}C NMR (100 MHz, $CDCl_3$) δ 20.1, 86.9, 98.5, 111.8, 119.7, 120.4, 122.8, 125.9, 128.9, 129.9, 130.88, 130.97, 132.6, 136.2, 137.5, 140.7; IR (KBr, cm^{-1}) $\tilde{\nu}$ = 741, 1250, 1335, 1458, 3379; UV (CH_3CN, nm) 204, 241, 293, 330 (sh); FL (CH_3CN, nm) 438; elemental analysis calcd (%) for $C_{32}H_{24}N_2 \cdot 0.10CHCl_3$: C, 85.97; H, 5.42; N, 6.25%; found: C, 86.06; H, 5.75; N, 6.25%; MS (LC-ESI-TOF, positive) m/z calcd for $C_{32}H_{25}N_2$: 436.1940 $[M]^+$; found: 436. 1941.

*1,2-Bis(2-(3-methoxyphenyl)-1H-indol-3-yl)ethyne (**1d**).* Yield, 385.2 mg (79%); R_f = 0.30 (hexane/EtOAc = 3/1); mp, 180.5−181.5 °C; ^1H NMR (400 MHz, acetone d_6) δ 3.79 (6H, s), 6.99 (2H, d, J = 10.0 Hz), 7.19−7.26 (4H, m), 7.43 (2H, t, J = 7.6 Hz), 7.49 (2H, d, J = 7.6 Hz), 7.91−7.95 (6H, m), 10.9 (2H, br-s); ^{13}C NMR (100 MHz, acetone d_6) δ 55.1, 88.8, 96.7, 111.9, 112.5, 114.2, 119.3, 120.1, 120.8, 123.6, 130.2, 130.9, 133.7, 136.5, 139.1, 160.6; IR (KBr, cm^{-1}) $\tilde{\nu}$ = 683, 741, 1045, 1219, 1458, 1558, 3394; UV (CH_3CN, nm) 213, 250, 313, 357; FL (CH_3CN, nm) 425, 452; elemental analysis calcd (%) for $C_{32}H_{24}N_2O_2 \cdot 0.05CHCl_3$: C, 81.12; H, 5.11; N, 5.90%; found: C, 80.39; H, 5.44; N, 6.01%; MS (LC-ESI-TOF, positive) m/z calcd for $C_{32}H_{26}N_2O_2$: 468.1838 $[M]^+$; found: 468.1806.

*3,3′-(Ethyne-1,2-diylbis(1H-indole-3,2-diyl))bis(N,N-dimethylaniline) (**1e**).* Yield, 437.2 mg (0.884 mmol), 85%; R_f = 0.30 (hexane/EtOAc = 3/1); mp, 221.5−222.5 °C; ^1H NMR (400 MHz, acetone d_6) δ 2.86 (12H, s), 6.77 (2H, dd, J = 2.4 and 8.4 Hz), 7.14−7.23 (4H, m), 7.30 (2H, t, J = 8.0 Hz), 7.46 (2H, d, J = 7.6 Hz), 7.61 (2H, d, J = 7.6 Hz), 7.74 (2H, s), 7.84 (2H, d, J = 7.6 Hz), 10.8 (2H, br-s); ^{13}C NMR

DOI: 10.1021/acs.joc.6b02668
J. Org. Chem. 2017, 82, 652−663

(100 MHz, acetone d_6) δ 40.0, 88.6, 96.2, 111.3, 111.8, 112.8, 115.1, 119.9, 120.6, 123.2, 129.6, 131.1, 133.0, 136.4, 140.4, 151.4; IR (KBr, cm^{-1}) $\tilde{\nu}$ = 737, 1246, 1508, 1601, 3394; UV (CH_3CN, nm) 206, 248, 311, 341 (sh); FL (CH_3CN, nm) 424, 443; elemental analysis calcd (%) for $C_{34}H_{30}N_4$: C, 82.56; H, 6.11; N, 11.33%; found: C, 82.26; H, 6.47; N, 11.2%; MS (LC-ESI-TOF, positive) m/z calcd for $C_{34}H_{32}N_4$: 494.2471 $[M]^+$; found: 494.2450.

*1,2-Bis(2-(4-(trifluoromethyl)phenyl)-1H-indol-3-yl)ethyne (**1f**).* Yield, 447.3 mg (79%); R_f = 0.30 (hexane/EtOAc = 5/1); mp, > 250 °C; ^{1}H NMR (400 MHz, acetone d_6) δ 7.24−7.33 (4H, m), 7.54 (2H, d, J = 8.0 Hz), 7.83 (4H, d, J = 8.0 Hz), 7.92 (2H, d, J = 7.6 Hz), 8.52 (4H, d, J = 8.0 Hz), 11.1 (2H, br-s); ^{13}C NMR (100 MHz, acetone d_6) δ 88.9, 98.0, 112.3, 120.2, 121.3, 124.3, 124.8 ($^1J_{C-F}$ = 269 Hz), 126.1 ($^3J_{C-F}$ = 4 Hz), 127.4, 129.4 ($^2J_{C-F}$ = 32 Hz), 130.6, 136.2, 136.9, 137.4; IR (KBr, cm^{-1}) $\tilde{\nu}$ = 748, 841, 1080, 1115, 1616, 3406; UV (CH_3CN, nm) 251, 318, 386, 469 (sh); FL (CH_3CN, nm) 456; elemental analysis calcd (%) for $C_{32}H_{18}F_6N_2$: C, 70.59; H, 3.33; F, 20.93; N, 5.14%; found: C, 70.55; H, 3.89; N, 5.15%; MS (LC-ESI-TOF, positive) m/z calcd for $C_{32}H_{19}F_6N_2$: 544.1374 $[M]^+$; found: 544.1351.

*1,2-Bis(2-(4-fluorophenyl)-1H-indol-3-yl)ethyne (**1g**).* Yield, 166.2 mg (36%); R_f = 0.30 (hexane/EtOAc = 4/1); mp, 238.0−239.0 °C; ^{1}H NMR (400 MHz, acetone d_6) δ 7.24−7.32 (8H, m), 7.49 (4H, d, J = 7.2 Hz), 7.86 (2H, d, J = 6.3 Hz), 8.33−8.36 (4H, m), 10.9 (2H, br-s); ^{13}C NMR (100 MHz, acetone d_6) δ 88.3, 96.5, 112.0, 116.0 ($^2J_{C-F}$ = 22 Hz), 119.9, 121.0, 123.6, 129.1, 129.2, 130.7, 136.6, 138.3, 162.9 ($^1J_{C-F}$ = 246 Hz); IR (KBr, cm^{-1}) $\tilde{\nu}$ = 741, 829, 1234, 1458, 1512, 3379; UV (CH_3CN, nm) 200, 250, 308, 364; FL (CH_3CN, nm) 418, 442; elemental analysis calcd (%) for $C_{30}H_{18}F_2N_2$: C, 81.07; H, 4.08; F, 8.55; N, 6.30%; found: C, 80.78; H, 4.63; N, 6.22%; MS (LC-ESI-TOF, positive) m/z calcd for $C_{30}H_{19}F_2N_2$: 444.1438 $[M]^+$; found: 444.1410.

*1,2-Bis(2-(3-fluorophenyl)-1H-indol-3-yl)ethyne (**1h**).* Yield, 171.0 mg (0.385 mmol), 37%; R_f = 0.30 (hexane/EtOAc = 4/1); mp, 239.0−240.0 °C; ^{1}H NMR (400 MHz, acetone d_6) δ 7.17−7.27 (6H, m), 7.49−7.58 (4H, m), 7.43 (2H, t, J = 7.6 Hz), 7.49 (2H, d, J = 7.6 Hz), 7.91−7.95 (6H, m), 11.0 (2H, br-s); ^{13}C NMR (100 MHz, acetone d_6) δ 89.1, 97.3, 112.1, 113.4 ($^2J_{C-F}$ = 23 Hz), 115.1 ($^2J_{C-F}$ = 21 Hz), 120.1, 121.1, 122.8 ($^4J_{C-F}$ = 2.7 Hz), 124.0, 130.7, 131.1 ($^3J_{C-F}$ = 8.4 Hz), 134.7 ($^3J_{C-F}$ = 8.5 Hz), 136.7, 137.7($^3J_{C-F}$ = 2.4 Hz), 163.5 ($^1J_{C-F}$ = 242 Hz); IR (KBr, cm^{-1}) $\tilde{\nu}$ = 671, 744, 779, 876, 1184, 1238, 1331, 1454, 1609, 3047, 3414; UV (CH_3CN, nm) 200, 253, 314, 376; FL (CH_3CN, nm) 430, 453; elemental analysis calcd (%) for $C_{30}H_{18}F_2N_2$: C, 81.07; H, 4.08; N, 6.30%; found: C, 80.63; H, 4.57; N, 6.33%; MS (LC-ESI-TOF, positive) m/z calcd for $C_{30}H_{19}F_2N_2$: 444.1438 $[M]^+$; found: 444.1459.

*1,2-Bis(2-(4-phenoxyphenyl)-1H-indol-3-yl)ethyne (**1i**).* Yield, 289.7 mg (47%); R_f = 0.30 (hexane/EtOAc = 4/1); mp, 219.5−220.5 °C; ^{1}H NMR (400 MHz, DMSO d_6) δ 7.10−7.25 (14H, m), 7.43 (4H, t, J = 8.4 Hz), 7.47 (2H, d, J = 8.0 Hz), 7.70 (2H, d, J = 7.6 Hz), 8.27 (4H, d, J = 8.8 Hz), 11.8 (2H, br-s); ^{13}C NMR (100 MHz, DMSO d_6) δ 88.2, 94.7, 111.9, 118.6, 118.9, 119.1, 120.4, 123.0, 124.0, 126.9, 128.4, 129.8, 130.2, 135.9, 138.2, 156.3, 156.9; IR (KBr, cm^{-1}) $\tilde{\nu}$ = 694, 741, 845, 1138, 1238, 1454, 1488, 1589, 3059, 3394, 3429; UV (CH_3CN, nm) 261, 312, 369; FL (CH_3CN, nm) 426, 449; elemental analysis calcd (%) for $C_{42}H_{28}N_2O_2$: C, 85.11; H, 4.76; N, 4.73; O, 5.40%; found: C, 84.80; H, 5.20; N, 4.73%; MS (LC-ESI-TOF, positive) m/z calcd for $C_{42}H_{30}N_2O_2$: 592.2151 $[M]^+$; found: 592.2122.

*1,2-Bis(2-(naphthalen-2-yl)-1H-indol-3-yl)ethyne (**1j**).* Yield, 289.7 mg (47%); R_f = 0.30 (hexane/EtOAc = 4/1); mp, >250 °C; ^{1}H NMR (400 MHz, DMSO d_6) δ 7.22 (2H, t, J = 7.2 Hz), 7.30 (2H, t, J = 7.6 Hz), 7.47−7.54 (4H, m), 7.56 (2H, d, J = 7.6 Hz), 7.81 (2H, d, J = 7.6 Hz), 7.85 (2H, d, J = 7.6 Hz), 7.94 (2H, d, J = 8.0 Hz), 8.02 (2H, d, J = 8.4 Hz), 8.51 (2H, d, J = 8.4 Hz), 8.82 (2H, s), 12.0 (2H, br-s); ^{13}C NMR (100 MHz, DMSO d_6) δ 88.7, 95.7, 112.1, 119.2, 120.6, 123.3, 124.6, 125.3, 126.6, 126.8, 127.8, 128.1, 128.4, 129.3, 130.0, 132.6, 133.1, 136.2, 138.6; IR (KBr, cm^{-1}) $\tilde{\nu}$ = 741, 821, 891, 1242, 1331, 1454, 3047, 3348, 3410; UV (CH_3CN, nm) 209, 248, 322, 379, 421 (sh); FL (CH_3CN, nm) 457, 475 (sh); elemental analysis calcd (%) for $C_{38}H_{24}N_2$: C, 89.74; H, 4.76; N, 5.51%; found: C, 89.43; H, 5.41; N, 5.40%; MS (LC-ESI-TOF, positive) m/z calcd for $C_{38}H_{25}N_2$: 508.1940 $[M]^+$; found: 508.1905.

*X-ray Crystal Analysis of **1a**.* The X-ray crystal structure was solved by direct methods (SIR-97)[29] and refined by full-matrix least-squares analysis (SHELXL-97)[30] using an isotropic extinction correction. All non-hydrogen atoms were refined anisotropically; hydrogen atoms were refined isotropically, whereby hydrogen positions are based on stereochemical considerations. CCDC-1505935 contains the supplementary crystallographic data (excluding structure factors) for this paper. These data can be obtained free of charge from The Cambridge Crystallographic Data Centre, 12 Union Road, Cambridge CB2 1EZ, UK (fax: + 44(1223)-336−033; e-mail: deposit@ccdc.cam.ac.uk), or via www.ccdc.cam.ac.Uk/data_request/cif. **1a**: Crystal data at 150 K for $C_{30}H_{20}N_2O_2$, $2(C_4H_8O_2)$, M_r = 584.27, monoclinic, space group $P21/a$, D_{calcd} = 1.227 g cm^{-3}, Z = 4, a = 7.0004(10) Å, b = 21.017(3) Å, c = 10.9249(17) Å, α = 90°, β = 100.0843°, γ = 120°, V = 1582.6 (4) Å^3; Mo Kα radiation, λ = 0.71070, μ = 0.079 mm^{-1}. A yellow crystal (linear dimensions ca. 0.50 × 0.45 × 0.30 mm) was obtained from EtOAc at 25 °C. Numbers of measured and unique reflections were 9298 and 3574, respectively (R_{int} = 0.0204). Final $R(F)$ = 0.0392, $wR(F^2)$ = 0.0952 for 205 parameters and 3574 reflections with $I > 2\sigma(I)$ (corresponding R values are 0.1034 for all data).

■ ASSOCIATED CONTENT

Supporting Information

The Supporting Information is available free of charge on the ACS Publications website at DOI: 10.1021/acs.joc.6b02668.

Crystallographic information (CIF)

NMR spectra, IR spectra, CVs, photophysical properties, X-ray crystal structures, theoretical methods, and additional references (PDF)

■ AUTHOR INFORMATION

Corresponding Authors

*E-mail: tshima@sun.it-chiba.ac.jp.

*E-mail: mitsuhiro.shibata@p.chibakoudai.jp.

ORCID

Toshiaki Shimasaki: 0000-0002-3447-7435

Notes

The authors declare no competing financial interest.

■ ACKNOWLEDGMENTS

We thank Dr. Yuki Yazawa of our university for the elemental analysis. We are also grateful to Dr. Shin-ichiro Kato of Gunma University for useful discussions with respect to the X-ray analysis and electrochemistry.

■ REFERENCES

(1) For recent reviews and books, see: (a) Shinoda, S. *Chem. Soc. Rev.* **2013**, *42*, 1825−1835. (b) Wang, F.; Wang, L.; Chen, X.; Yoon, J. *Chem. Soc. Rev.* **2014**, *43*, 4312−4324. (c) Patra, S.; Maity, D.; Gunupuru, R.; Agnihotri, P.; Paul, P. *J. Chem. Sci.* **2012**, *124*, 1287−1299.

(2) For recent reviews, see: (a) Anthony, J. E. *Chem. Rev.* **2006**, *106*, 5028−5048. (b) Wang, C.; Dong, H.; Hu, W.; Liu, Y.; Zhu, D. *Chem. Rev.* **2012**, *112*, 2208−2267.

(3) For recent reviews, see: (a) Li, D.; Zhang, H.; Wang, Y. *Chem. Soc. Rev.* **2013**, *42*, 8416−8433. (b) Zhu, M.; Yang, C. *Chem. Soc. Rev.* **2013**, *42*, 4963−4976. (c) Chen, S.; Wu, Q.; Kong, M.; Zhao, X.; Yu, Z.; Jia, P.; Huang, W. *J. Mater. Chem. C* **2013**, *1*, 3508−3524. (d) Jiang, H. *Asian J. Org. Chem.* **2014**, *3*, 102−112.

(4) For recent reviews and books, see: (a) Balzani, V.; Credi, A.; Venturi, M. *Molecular Devices and Machines*; Wiley-VCH: New York, 2004; Chapter 6. (b) Günes, S.; Neugebauer, H.; Sariciftci, N. S. *Chem.*

DOI: 10.1021/acs.joc.6b02668
J. Org. Chem. 2017, 82, 652−663

Rev. **2007**, *107*, 1324−1338. (c) Cheng, P.; Zhan, X. *Chem. Soc. Rev.* **2016**, *45*, 2544−2582.
(5) For examples, see: (a) Figueira-Duarte, T. M.; Müllen, K. *Chem. Rev.* **2011**, *111*, 7260−7314. (b) Zhang, L.; Hughes, D. L.; Cammidge, A. N. *J. Org. Chem.* **2012**, *77*, 4288−4297.
(6) For recent reviews and books, see: (a) Toyota, S.; Iwanaga, T. *Top. Curr. Chem.* **2012**, *350*, 111−140. (b) Spitler, E. L.; Johnson, C. A., II; Haley, M. M. *Chem. Rev.* **2006**, *106*, 5344−5386. (c) Müller, T. J. J.; Bunz, U. H. F. *Functional Organic Materials*; Wiley-VCH: New York, 2007; Chapter 6.
(7) For examples, see: (a) Zang, L.; Che, Y.; Moore, J. S. *Acc. Chem. Res.* **2008**, *41*, 1596−1608. (b) Tahara, K.; Lei, S.; Adisoejoso, J.; De Feyter, S.; Tobe, Y. *Chem. Commun.* **2010**, *46*, 8507−8525. (c) Hisaki, I.; Sonoda, M.; Tobe, Y. *Eur. J. Org. Chem.* **2006**, *2006*, 833−847. (d) Terao, J.; Wadahama, A.; Matono, A.; Tada, T.; Watanabe, S.; Seki, S.; Fujihara, T.; Tsuji, Y. *Nat. Commun.* **2013**, *4*, 1691−1699. (e) Aggarwal, A. V.; Thiessen, A.; Idelson, A.; Kalle, D.; Würsch, D.; Stangl, T.; Steiner, F.; Jester, S.-S.; Vogelsang, J.; Höger, S.; Lupton, J. M. *Nat. Chem.* **2013**, *5*, 964−970. (f) Kato, S.-i.; Yamada, Y.; Hiyoshi, H.; Umezu, K.; Nakamura, Y. *J. Org. Chem.* **2015**, *80*, 9076−9090.
(8) Zhao, C.-H.; Wakamiya, A.; Inukai, Y.; Yamaguchi, S. *J. Am. Chem. Soc.* **2006**, *128*, 15934−15935.
(9) (a) Wilson, J. N.; Bunz, U. H. F. *J. Am. Chem. Soc.* **2005**, *127*, 4124−4125. (b) Coluccini, C.; Sharma, A. K.; Caricato, M.; Sironi, A.; Cariati, E.; Righetto, S.; Tordin, E.; Botta, C.; Forni, A.; Pasini, D. *Phys. Chem. Chem. Phys.* **2013**, *15*, 1666−1674. (c) Caricato, M.; Coluccini, C.; Griend, D. A. V.; Forni, A.; Pasini, D. *New J. Chem.* **2013**, *37*, 2792−2799.
(10) Jegou, G.; Jenekhe, S. A. *Macromolecules* **2001**, *34*, 7926−7928.
(11) For recent reviews and books, see: (a) Juwarker, H.; Jeong, K.-S. *Chem. Soc. Rev.* **2010**, *39*, 3664−3674. (b) Juwarker, H.; Suk, J.-m.; Jeong, K.-S. *Chem. Soc. Rev.* **2009**, *38*, 3316−3325. (c) Kawase, T. *Synlett* **2007**, *17*, 2609−2626. (d) Kawase, T.; Kurata, H. *Chem. Rev.* **2006**, *106*, 5250−5273. (e) Nielsen, M. B.; Diederich, F. *Chem. Rev.* **2005**, *105*, 1837−1867. (f) Schrader, T.; Hamilton, A. D. *Functional Synthetic Receptors*; Wiley-VCH: New York, 2005.
(12) Kawase, T.; Fujiwara, N.; Tsutumi, M.; Oda, M.; Maeda, Y.; Wakahara, T.; Akasaka, T. *Angew. Chem., Int. Ed.* **2004**, *43*, 5060−5062.
(13) For examples, see: (a) Crich, D.; Banerjee, A. *Acc. Chem. Res.* **2007**, *40*, 151−161. (b) Kochanowska-Karamyan, A. J.; Hamann, M. T. *Chem. Rev.* **2010**, *110*, 4489−4497.
(14) For examples, see: (a) Lo, K. K.-W.; Tsang, K. H.-K.; Sze, K.-S.; Chung, C.-K.; Lee, T. K.-M.; Zhang, K. Y.; Hui, W.-K.; Li, C.-K.; Lau, J. S.-Y.; Ng, D. C.-M.; Zhu, N. *Coord. Chem. Rev.* **2007**, *251*, 2292−2310. (b) Vasil'ev, R. F.; Trofimov, A. V.; Tsaplev, Y. B. *Russ. Chem. Rev.* **2010**, *79*, 77−88.
(15) For recent reviews, see: (a) Cacchi, S.; Fabrizi, G. *Chem. Rev.* **2011**, *111*, PR215−PR287. (b) Shiri, M. *Chem. Rev.* **2012**, *112*, 3508−3549. (c) Platon, M.; Amardeil, R.; Djakovitch, L.; Hierso, J.-C. *Chem. Soc. Rev.* **2012**, *41*, 3929−3968. (d) Humphrey, G. R.; Kuethe, J. T. *Chem. Rev.* **2006**, *106*, 2875−2911. (e) Nitti, A.; Signorile, M.; Boiocchi, M.; Bianchi, G.; Po, R.; Pasini, D. *J. Org. Chem.* **2016**, *81*, 11035−11042.
(16) Jang, Y. H.; Youn, S. W. *Org. Lett.* **2014**, *16*, 3720−3723.
(17) Nenajdenko, V. G. *Isocyanide Chemistry*; Wiley-VCH: New York, 2012; Chapter 2.
(18) Suginome, M.; Fukuda, T.; Ito, Y. *Org. Lett.* **1999**, *1*, 1977−1979.
(19) (a) Liu, L.; Wang, Y.; Wang, H.; Peng, C.; Zhao, J.; Zhu, Q. *Tetrahedron Lett.* **2009**, *50*, 6715−6719. (b) Mitamura, T.; Nomoto, A.; Sonoda, M.; Ogawa, A. *Bull. Chem. Soc. Jpn.* **2010**, *83*, 822−824. (c) Lu, X.; Petersen, J. L.; Wang, K. K. *Org. Lett.* **2003**, *5*, 3277−3280. (d) Mitamura, T.; Ogawa, A. *J. Org. Chem.* **2011**, *76*, 1163−1166.
(20) Metal-catalyzed cyclization reactions of arylisocyanides have been reported as follows: (a) Onitsuka, K.; Segawa, M.; Takahashi, S. *Organometallics* **1998**, *17*, 4335−4337. (b) Kamijo, S.; Yamamoto, Y. *J. Am. Chem. Soc.* **2002**, *124*, 11940−11945. (c) Tobisu, M.; Fujihara, H.; Koh, K.; Chatani, N. *J. Org. Chem.* **2010**, *75*, 4841−4847.
(21) 1,2-Bis(1*H*-indol-3-yl)ethyne **8** and its derivatives have been investigated mainly as the synthetic intermediates of indolocarbazole alkaloids so far: (a) Fu, L.; Gribble, G. W. *Tetrahedron Lett.* **2010**, *51*, 537−539. (b) Roy, S.; Gribble, G. W. *Synth. Commun.* **2007**, *37*, 829−837. (c) Prateeptongkum, S.; Driller, K. M.; Jackstell, R.; Spannenberg, A.; Beller, M. *Chem. - Eur. J.* **2010**, *16*, 9606−9615. (d) Oakdale, J. S.; Boger, D. L. *Org. Lett.* **2010**, *12*, 1132−1134.
(22) Capelli, L.; Crescenzi, O.; Manini, P.; Pezzella, A.; Barone, V.; d'Ischia, M. *J. Org. Chem.* **2011**, *76*, 4457−4466.
(23) Frisch, M. J.; Trucks, G. W.; Schlegel, H. B.; Scuseria, G. E.; Robb, M. A.; Cheeseman, J. R.; Scalmani, G.; Barone, V.; Mennucci, B.; Petersson, G. A.; Nakatsuji, H.; Caricato, M.; Li, X.; Hratchian, H. P.; Izmaylov, A. F.; Bloino, J.; Zheng, G.; Sonnenberg, J. L.; Hada, M.; Ehara, M.; Toyota, K.; Fukuda, R.; Hasegawa, J.; Ishida, M.; Nakajima, T.; Honda, Y.; Kitao, O.; Nakai, H.; Vreven, T.; Montgomery, J. A. Jr.; Peralta, J. E.; Ogliaro, F.; Bearpark, M.; Heyd, J. J.; Brothers, E.; Kudin, K. N.; Staroverov, V. N.; Kobayashi, R.; Normand, J.; Raghavachari, K.; Rendell, A.; Burant, J. C.; Iyengar, S. S.; Tomasi, J.; Cossi, M.; Rega, N.; Millam, J. M.; Klene, M.; Knox, J. E.; Cross, J. B.; Bakken, V.; Adamo, C.; Jaramillo, J.; Gomperts, R.; Stratmann, R. E.; Yazyev, O.; Austin, A. J.; Cammi, R.; Pomelli, C.; Ochterski, J. W.; Martin, R. L.; Morokuma, K.; Zakrzewski, V. G.; Voth, G. A.; Salvador, P.; Dannenberg, J. J.; Dapprich, S.; Daniels, A. D.; Farkas, Ö.; Foresman, J. B.; Ortiz, J. V.; Cioslowski, J.; Fox, D. J. *Gaussian 09*, revision B.01; Gaussian, Inc., Wallingford, CT, 2010.
(24) Klukas, F.; Grunwald, A.; Menschel, F.; Müller, T. J. J. *Beilstein J. Org. Chem.* **2014**, *10*, 672−679.
(25) (a) Pommerehne, J.; Vestweber, H.; Guss, W.; Mahrt, R. F.; Bassler, H.; Porsch, M.; Daub, J. *Adv. Mater.* **1995**, *7*, 551−554. (b) Chi, C.; Wegner, G. *Macromol. Rapid Commun.* **2005**, *26*, 1532−1537.
(26) Toyota, S. *Chem. Rev.* **2010**, *110*, 5398−5424.
(27) Lin, C. I.; Selvi, S.; Fang, J.-M.; Chou, P.-T.; Lai, C.-H.; Cheng, Y.-M. *J. Org. Chem.* **2007**, *72*, 3537−3542.
(28) Evans, L. A.; Petrovic, M.; Antonijevic, M.; Wiles, C.; Watts, P.; Wadhawan, J. *J. Phys. Chem. C* **2008**, *112*, 12928−12935.
(29) Altomare, A.; Burla, M. C.; Camalli, M.; Cascarano, G. L.; Giacovazzo, C.; Guagliardi, A.; Moliterni, A. G. G.; Polidori, G.; Spagna, R. *J. Appl. Crystallogr.* **1999**, *32*, 115−119.
(30) Sheldrick, G. M. *SHELXL-97, Program for the Refinement of Crystal Structures*; University of Göttingen: Germany, 1997.

DOI: 10.1021/acs.joc.6b02668
J. Org. Chem. 2017, 82, 652−663